The Nucleus ***62***, *No. 1 (2025) 37-46*

https://doi.org/10.71330/thenucleus.2025.1445

www.thenucleuspak.org.pk

The Nucleus

ISSN 0029-5698 (Print)

ISSN 2306-6539 (Online)

DFT-Based Quantum Chemical Analysis of Coumarin Derivatives

Srinath More*, Omnath Patil, Shivakumar Chillargikar, Dayanand Lalasangi and S. M. Hanagodimath

Department of PG Studies and Research in Physics, Gulbarga University, Kalaburagi – 585 106, Karnataka, India.

ABSTRACT

The goal of the current work is to use density functional theory (DFT) at the B3LYP level of theory, using a basis set of 6-311++G (d, p), to comprehend the physical and chemical characteristics of 6-Methoxy-4-(4-nitro-phenoxy methyl)-chromen-2-one (6MNPM) and 1-(4-nitro-phenoxy methyl)-benzo[f]-chromen-3-one (4NPMB) of coumarin derivatives. Bond lengths and bond angles, two geometrical parameters, are calculated for coumarin derivatives. We have estimated the frontier molecular orbitals (FMO). Furthermore, to shed light on the stability and chemical reactivity of coumarin derivatives, the global reactivity descriptors were computed using FMO. The molecular electrostatic potential (MEP) investigation aims to identify the coumarin molecules' preferred locations for electrophilic and nucleophilic attacks. The distribution of atomic charge in Mulliken has been performed. The nonlinear optical properties (NLO) of coumarin molecules have been calculated to assess their suitability for NLO applications. The computation of natural bonding orbital (NBO) allows the identification of the most likely intense intermolecular interactions. The analysis focused on the temperature dependency of the thermodynamic characteristics of coumarin derivatives.

Keywords: *Frontier molecular orbitals (FMO), Nonlinear optical properties (NLO), Molecular electrostatic potential (MEP), and thermodynamic parameters.*

1. Introduction

Coumarin is a versatile scaffold with intriguing biological, pharmacological, biochemical, medicinal, and photochemical properties, offering various applications [1-4]. It belongs to the benzopyrone family and is produced when a benzene ring and an α-pyrone ring fuse together. Since A. Vogel discovered coumarin from tonka beans in 1820, the compound has been identified in seeds, roots, and leaves, particularly among green plants [5]. The coumarin molecule (2H-chromen-2-one) can exhibit a broad spectrum of pharmacological activity because it interacts with numerous important sites in organisms in many ways through multiple mechanisms, including hydrophobic interactions, hydrogen bonding, and electrostatic interactions [6]. Additionally, coumarin derivatives are produced for various uses, such as dye lasers and solar cells with dye sensitization [7]. Furthermore, by replacing the aromatic ring, the versatile function of coumarin allows for adaptable structural changes in the scaffold position (3 and 4) [8]. Phenyl-coumarins are synthetically versatile derivatives that have shown biological and pharmacological effects with an additional phenyl ring connected to any position of the coumarin scaffold. They are regarded as a key class of molecular moiety [9]. Computational techniques can offer useful molecular details for these coumarin derivatives. Consequently, the main goal of this work is to determine the link between the calculated molecular characteristics and the chemical substitutions by examining the structure, electrical, and optical properties of these identical derivatives [10]. We utilized density functional theory (DFT) [11], which is a widely and extensively used quantum mechanical technique, to compute the electronic and structural characteristics of the derivatives [12–14].

The two coumarin derivatives were subjected to a thorough computer analysis [15]. The molecular characteristics of coumarin derivatives have been the subject of several computational DFT investigations for use in optoelectronics [16,17], solar cells [18–21], fluorescent dyes, and lasers [22]. The motivation behind this work is to understand the basic properties of coumarin derivatives with the help of a computational approach, and the results are useful for synthesizing new substitutes of the coumarin molecule, which are useful for optoelectronic devices, sensing applications, and as drug carriers in the medical field. The presented work has not been carried out on the 6MNPM and 4NPMB coumarin derivatives.

2. Materials and methods

2.1. Materials

6-Methoxy-4-(4-nitro-phenoxy methyl)-chromen-2-one (6MNPM) and 1-(4-nitro-phenoxy methyl)-benzo[f]-chromen-3-one (4NPMB) coumarin derivatives were synthesized as per the procedure reported in the literature [23]. The composition of the compounds of the coumarin derivatives is given in Fig. 1 (a) and (b).

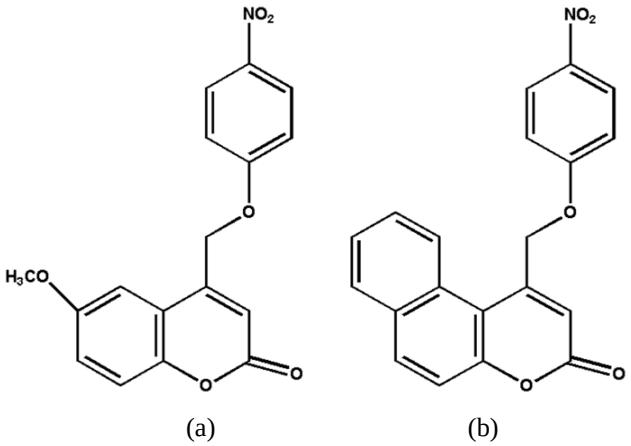

(a) (b)

Fig. 1 Molecular structures of (a) 6MNPM and (b) 4NPMB molecules

2.2. Quantum Computational details

The DFT approach has been utilized to accomplish the quantum chemical computation of coumarin derivatives at

*Corresponding author: srinathmore@gmail.com

the B3LYP model, with a basis set of 6-311++G (d, p). Gaussian 16 software is used to compute the various properties of the specified derivatives [24]. All computations have been performed to better address the polar bonds of the methoxy and nitro groups. The triple split valence basis set 6-311++G is expanded by including the polarization function (p) and diffuse function (d) for heavy atoms. In the gas phase, the optimization was carried out. The improved geometry has been utilized for the subsequent computations [25-28].

3. Results and Discussion

3.1 Geometrical parameters

The 6MNPM and 4NPMB are substituted phenoxymethyl with two different functional groups: nitro (NO2), methoxy (CH3O), and nitro (NO2), and benzo[f] chromene-3-one (an extra benzene ring to the coumarin). The mentioned functional groups are planar to the benzene ring. Using a basic set of 6-311G++ (d, p), the geometrical parameters, such as the bond length and bond angle of derivatives, were optimized at B3LYP using the DFT approach. As seen in Fig. 2 (a-b), the optimal molecular geometry was calculated at the theoretical level of B3LYP. According to the computed summary of the derivatives' optimal structure, they are members of the C1 point group. The dipole moments of 6MNPM and 4NPMB derivatives in the ground state are 3.44D and 5.15D, respectively. This indicates that the molecule's polarity increases from 6MNPM to 4NPMB molecules. By using the mentioned method, the geometrical characteristics of coumarin derivatives were derived from the optimized molecular structure and are shown in Table 1 (a-b). The parameters, like bond length, bond angle, and dihedral angle, show similar values in both molecules.

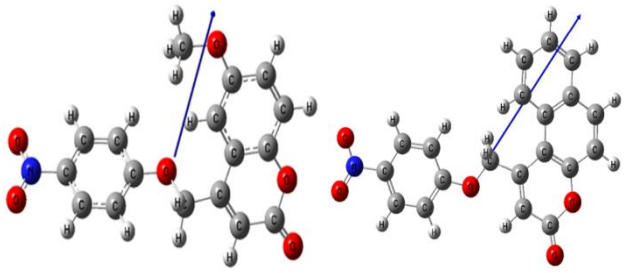

(a) (b)

Fig. 2 Optimized geometries with dipole moment vector of (a) 6MNPM and (b) 4NPMB molecules.

3.2 Frontier molecular orbital (FMO)

A frontier molecular orbital (FMO) is the intersection of the lowest unoccupied molecular orbital (LUMO) and the highest occupied molecular orbital (HOMO) [29–31]. For coumarin derivatives, the HOMO and LUMO energy plots together with the band gap energy were calculated at B3LYP of DFT using the basis set of 6-311++G (d, p). Figure 3 (a-b) present the electron energy distribution in the HOMO and LUMO for the coumarin derivatives. The observation from Figure 3 (a-b) is, that in the 6MNPM and 4NPMB derivatives for LUMO, the phenoxy methyl and the functional group of the molecule, NO_2 occupies electron density. Whereas in HOMO the localization of electron density is on the methoxy which is attached to the benzene ring but there is a slight change in the distribution of electron density in both derivatives due to the role played by the functional groups attached to the aromatic ring. This indicates the possible intermolecular charge transfer. To examine the chemical reactivity, hardness (η), softness (S), electronegativity (χ), potential (μ), ionization potential (I), electron affinity (E), energy gap (E_g), and electrophilicity index (ω) of derivatives, it is essential to obtain the HOMO-LUMO energy gap value [32, 33]. Using Koopman's formulas, these parameters were determined for the coumarin derivatives in the chemical model, and the obtained values are listed in Table 2. The energy gap in the examined derivatives reduces in the following order: 6MNPM < 4NPMB molecule. This suggests that the energy gap of the 6MNPM molecule is lower. In comparison to the 4NPMB, the 6MNPM molecule has a lower energy value, which suggests that it is more chemically soft, highly reactive, and has weak kinetic stability. Electron affinity (E) and electronegativity (χ) will give information about the electron-accepting ability of a molecule; the higher the values of (E) and (χ), the better the electron-accepting ability. 6MNPM and 4NPMB derivatives have the same value. This means that both derivatives can accept electrons from computational quantum calculations. The electrophilicity index further clarifies the system's capacity for accepting electrons; a higher value of it indicates a higher electron-accepting ability of the molecule. 6MNPM and 4NPMB have very small changes in the value of the electrophilicity index of 0.01 between them, so on this basis, 6MNPM has a higher electron-accepting ability compared to the 4NPMB molecule.

Table 1 (a). Optimized geometrical parameters of 6MNPM molecules.

Structural parameters	B3LYP / 6-311++G (d, p)
Bond length (A^0)	
C1-C5	1.5
C1-O14	1.4
C2-C3	1.3
C3-C4	1.5
C4-C5	1.3
C5-H9	1.0
C7-C11	1.3
C21-O22	1.4
C23-C28	1.3
C24-C25	1.3
C26-N33	1.4
N33-O34	1.1
N33-O35	1.3
Bond angle (θ)	
C5-C1-C14	120.7
O14-C1-O15	119.6
C3-C2-O14	122.3

C2-C3-C4	120.6
C3-C4-C5	118.5
C10-C8-H12	119.9
C8-C10-C11	119.9
O22-C21-H36	109.4
O22-C23-C24	120.0
C24-C23-C28	120.0
C26-N33-O34	120.0
O34-N33-O35	120.0
Dihedral angle (θ)	
O14-C1-C5-C4	010.4
O14-C1-C5-H9	-170.0
O15-C1-C5-H9	009.2
C5-C1-O14-C2	-022.5
O15-C1-O14-C2	158.0
O14-C2-C7-H6	003.9
O14-C2-C7-C11	-175.7
C3-C2-O14-C1	020.7
O22-C23-C24-H30	000.0
C28-C23-C24-H25	000.0
C28-C23-C24-H30	-180.0

Table 1 (b). Optimized geometrical parameters of 4NPMB molecules.

Structural parameter	B3LYP/6-311++G(d, p)
Bond length (A^0)	
C1-C2	1.5
C1-C6	1.3
C1-H18	1.0
C2-C3	1.3
C2-H19	1.0
C3-C4	1.5
C3-H35	1.0
C4-C5	1.3
C4-C7	1.5
C5-C6	1.5
C6-H20	1.0
C7-C8	1.5
C7-C13	1.3
Bond angle (θ)	
C2-C1-C6	119.9
C2-C1-H18	120.0
C6-C1-H18	120.0
C1-C2-C3	119.9
C1-C2-H19	120.0
C3-C2-H19	120.0
C2-C3-C4	120.0
C2-C3-H35	119.9
C4-C3-H35	119.9
C3-C4-C5	119.9
C3-C4-C7	119.9
C5-C4-C7	120.1
Dihedral angle (θ)	
C6-C1-C2-C3	000.0
C6-C1-C2-C19	-179.9
H18-C1-C2-C3	-179.9
H18-C1-C2-H19	000.0
C2-C1-C6-C5	-0.060
C2-C1-C6-H20	179.9
H18-C1-C6-C5	179.9
H18-C1-C6-H20	-0.058
C1-C2-C3-H35	-179.9
C1-C2-C3-H35	-179.9
H19-C2-C3-C4	-179.9

Table 2. Calculated energy values of global reactivity descriptors of 6MNPM and 4NPMB molecules by B3LYP/6-311++G (d, p) method.

Parameters with Unit	DFT	
	6MNPM	4NPMB
E_{HOMO} (eV)	-0.22815	-0.23039
E_{LUMO} (eV)	-0.08895	-0.08659
Energy gap (E_g) (eV)	0.13920	0.14380
Ionization potential (I) (eV)	0.22815	0.23039
Electron affinity (E) (eV)	0.08895	0.08659
Electronegativity (χ) (eV)	0.15855	0.15849
Chemical potential (μ) (eV)	-0.15855	-0.15849
Chemical hardness (η) (eV)	0.06960	0.07190
Chemical softness (S) (eV^{-1})	14.36781	13.90820
Electrophilicity index (ω) (eV)	0.18053	0.17461

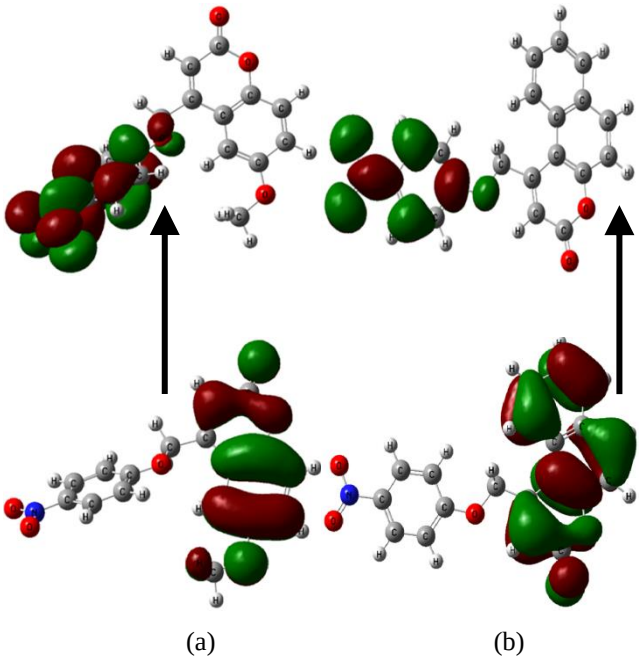

(a) (b)

Fig 3. HOMO and LUMO of (a) 6MNPM and (b) 4NPMB molecules.

3.3 Molecular Electrostatic Potential (MEP)

The molecular electrostatic potential(MEP) is utilized to show the hydrogen bonding interactions and it describes a molecule's nucleophilic and electrophilic sites qualitatively

[32, 34]. The physio-chemical characteristics are also analyzed using MEP. The MEP color coding goes as follows: red denotes an electron-rich site, which is the spot where an electrophilic attack is more likely to occur. Yellow denotes a little electron deficiency, green denotes neutrality, light blue denotes a slight electron deficiency, and blue denotes an electron deficiency, the ideal location for a nucleophilic attack. These maps provide us with the ability to see a molecule's variable charge areas. The present study obtains the 3-dimensional plot of MEP of coumarin derivatives using the DFT model. The MEP maps obtained from chemical mode have certain similarities. Fig. 4 (a-b) shows the MEP-mapped surface estimated for coumarin derivatives at the B3LYP level of theory. This sort of circumstance has been observed in various compounds. It is referred to as electrophilic attack because it demonstrates that negative potential is dispersed around the oxygen atom that is linked to the carbon [35], with potential elevations in the following order: red, orange, green, and blue. In the 6MNPM molecule, the color coding of these maps falls between -0.0544 a.u. (deepest red) and 0.0544 a.u. (deepest blue). The nitrogen N and hydrogen H atoms connected to the benzene ring are surrounded by a positive potential, making this an attractive target for nucleophilic attack. When contrasted, the N atoms' positive potential value is 0.011 a.u, and the H atoms also have a positive potential value of identical magnitude. However, the H atom has a larger positive potential than the N atom. Concerning the H atoms in the CH_3 group, the maximal positive areas have a value of 0.031 a.u. In contrast, the 6MNPM molecule's H atoms in the ring have smaller values than those at the CH_3. As a result, the electrostatic potential distribution of 4NPMB and its surrounding molecule is somewhat altered when a benzene ring is added in place of a methyl group in the provided molecule. Coumarin derivatives exhibit chemical activity due to the presence of both nucleophilic and electrophilic attack sites.

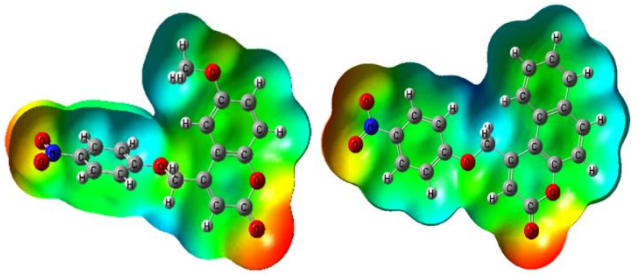

(a) (b)

Fig. 4 Electrostatic Density Surface of (a) 6MNPM and (b) 4NPMB molecules.

3.4 Mulliken Atomic Charges

Using a quantum chemistry approach, the Mullikan atomic charge analysis may be performed to characterize the impacts of atomic charge, dipole moment, electronic structure and molecule polarizability of the system [36, 35]. The Mulliken atomic charge distribution of the derivatives is computed at the B3LYP level of theory using the DFT chemical model, employing the basis set of 6-311++G (d, p) for the coumarin molecules. Figures 5 (a, b) show the distribution of atomic charges in Mulliken for coumarin molecules. The distribution of charge between the 6MNPM and 4NPMB derivatives is found to differ noticeably. In the molecule of 6MNPM, the C_1 atom has a charge of 0.5922C and it is surrounded by the carbon and hydrogen atoms and attached by oxygen atoms. The 4NPMB molecule also consists of a C_1 atom with a charge of -0.0864 C. It is in the aromatic ring and connected by the H atom. So here clearly, we can see the difference in the charge occupied by the C_1 atom. This could be due to the conjugation interaction between the C1 and its surrounding atoms.

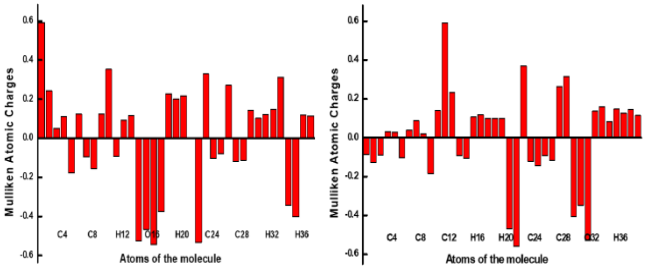

(a) (b)

Fig 5. Mulliken Atomic Charge Distribution of (a) 6MNPM and (b) 4NPMB molecules.

3.5 Natural Bond Orbital Analysis (NBO)

Natural bond orbital analysis (NBO) was used to interpret interaction atomic orbitals on title molecules, revealing atomic charges, orbital occupancies, hybrid contributions, and electron density delocalization. The NAO orbital energies are calculated by using the Kohu-sham operator (F) as

$$\varepsilon_i^{(A)} = \langle \theta_i^{(A)} / F / \theta_i^{(A)*} \rangle$$

Table 3 (a-b) depict many bonding principles, such as the kind of bond orbital, occupancies, natural atomic hybrids that comprise the NBO, and the proportion of each hybrid in the NBO. Furthermore, the hybrid label and atom label show the quantity of s-character, p-character and additional hybrid orbital (sp_x) composition of coumarin molecules, as estimated by the B3LYP/6-311++G (d, p) basis set using DFT as a chemical model [37–41]. Table 4 (ab) summarizes the stabilizing energy of several types of interaction. As shown below, the stabilization energy E (2) is connected to the delocalization of i (donor) → j (acceptor) [42, 43].

$$E^{(2)} = -q_i \frac{F^2(i,J)}{\varepsilon_j - \varepsilon_i}$$

Table 3(a). Natural bond orbital analysis of 6MNPM molecule by DFT/B3LYP with the basic set 6-311++G (d, p).

Bond orbital	Occupancy	Atom	Contribution from parent NBO (%)	Atomic hybrid contribution (%)
σC1-C2	1.97984	C1	49.94	S(30.92)+P(69.04)+D(0.04)
		C2	50.06	S(30.83)+P(69.13)+D(0.04)
πC1-C6	1.82588	C1	50.09	S(00.00)+P(99.94)+D(0.06)
		C6	49.91	S(00.00)+P(99.94)+D(0.06)
πC2-C3	1.83272	C2	48.25	S(00.00)+P(99.94)+D(0.06)
		C3	51.75	S(00.00)+P(99.96)+D(0.04)
πC4-C5	1.70412	C4	50.06	S(00.00)+P(99.95)+D(0.05)
		C5	49.94	S(00.00)+P(99.95)+D(0.05)
πC7-C13	1.76916	C7	52.80	S(00.00)+P(99.95)+D(0.05)
		C13	47.20	S(00.01)+P(99.92)+D(0.07)
πC8-C10	1.84714	C8	48.06	S(00.07)+P(99.86)+D(0.07)
		C10	51.94	S(00.06)+P(99.87)+D(0.07)
πC12-O21	1.98014	C12	32.29	S(00.26)+P(99.58)+D(0.16)
		O21	67.71	S(00.15)+P(99.56)+D(0.29)
πC14-C15	1.83286	C14	51.05	S(00.00)+P(99.94)+D(0.06)
		C15	48.95	S(00.00)+P(99.94)+D(0.06)
πC23-C25	1.77184	C23	47.43	S(00.01)+P(99.92)+D(0.07)
		C25	52.57	S(00.00)+P(99.94)+D(0.06)
σ*C1-C2	0.02155	C1	50.06	S(30.92)+P(69.04)+D(0.04)
		C2	49.94	S(30.83)+P(69.13)+D(0.04)
π*C1-C6	0.15664	C1	49.91	S(00.00)+P(99.94)+D(0.06)
		C6	50.09	S(00.00)+P(99.94)+D(0.06)
π*C2-C3	0.17183	C2	51.75	S(00.00)+P(99.94)+D(0.06)
		C3	48.25	S(00.00)+P(99.96)+D(0.04)
π*C4-C5	0.30175	C4	49.94	S(00.00)+P(99.95)+D(0.05)
		C5	50.06	S(00.00)+P(99.95)+D(0.05)
π*C7-C13	0.27597	C7	47.20	S(00.00)+P(99.95)+D(0.05)
		C13	52.80	S(00.01)+P(99.92)+D(0.07)
π*C8-C10	0.12327	C8	51.94	S(00.07)+P(99.86)+D(0.07)
		C10	48.06	S(00.06)+P(99.87)+D(0.07)
π*C12-O21	0.24436	C12	67.71	S(00.06)+P(99.58)+D(0.16)
		O21	32.29	S(00.15)+P(99.56)+D(0.29)
π*C14-C15	0.15948	C14	48.95	S(00.00)+P(99.94)+D(0.06)
		C15	51.05	S(00.00)+P(99.94)+D(0.06)
π*C23-C25	0.23609	C23	52.57	S(00.01)+P(99.92)+D(0.07)
		C25	47.43	S(00.00)+P(99.94)+D(0.06)

Table 3(b). Natural bond orbital analysis of 4NPMB molecule by DFT/B3LYP with the basic set 6-311++G (d, p).

Bond orbital	Occupancy	Atom	Contribution from parent NBO (%)	Atomic hybrid contribution (%)
σC1-C2	1.97984	C1	49.94	S(30.92)+P(69.04)+D(0.04)
		C2	50.06	S(30.83)+P(69.13)+D(0.04)
πC1-C6	1.82588	C1	50.09	S(00.00)+P(99.94)+D(0.06)
		C6	49.91	S(00.00)+P(99.94)+D(0.06)
πC2-C3	1.83272	C2	48.25	S(00.00)+P(99.94)+D(0.06)
		C3	51.75	S(00.00)+P(99.96)+D(0.04)
πC4-C5	1.70412	C4	50.06	S(00.00)+P(99.95)+D(0.05)
		C5	49.94	S(00.00)+P(99.95)+D(0.05)
πC7-C13	1.76916	C7	52.80	S(00.00)+P(99.95)+D(0.05)
		C13	47.20	S(00.01)+P(99.92)+D(0.07)
πC8-C10	1.84714	C8	48.06	S(00.07)+P(99.86)+D(0.07)

		C10	51.94	S(00.06)+P(99.87)+D(0.07)
πC12-O21	1.98014	C12	32.29	S(00.26)+P(99.58)+D(0.16)
		O21	67.71	S(00.15)+P(99.56)+D(0.29)
πC14-C15	1.83286	C14	51.05	S(00.00)+P(99.94)+D(0.06)
		C15	48.95	S(00.00)+P(99.94)+D(0.06)
πC23-C25	1.77184	C23	47.43	S(00.01)+P(99.92)+D(0.07)
		C25	52.57	S(00.00)+P(99.94)+D(0.06)
σ*C1-C2	0.02155	C1	50.06	S(30.92)+P(69.04)+D(0.04)
		C2	49.94	S(30.83)+P(69.13)+D(0.04)
π*C1-C6	0.15664	C1	49.91	S(00.00)+P(99.94)+D(0.06)
		C6	50.09	S(00.00)+P(99.94)+D(0.06)
π*C2-C3	0.17183	C2	51.75	S(00.00)+P(99.94)+D(0.06)
		C3	48.25	S(00.00)+P(99.96)+D(0.04)
π*C4-C5	0.30175	C4	49.94	S(00.00)+P(99.95)+D(0.05)
		C5	50.06	S(00.00)+P(99.95)+D(0.05)
π*C7-C13	0.27597	C7	47.20	S(00.00)+P(99.95)+D(0.05)
		C13	52.80	S(00.01)+P(99.92)+D(0.07)
π*C8-C10	0.12327	C8	51.94	S(00.07)+P(99.86)+D(0.07)
		C10	48.06	S(00.06)+P(99.87)+D(0.07)
π*C12-O21	0.24436	C12	67.71	S(00.06)+P(99.58)+D(0.16)
		O21	32.29	S(00.15)+P(99.56)+D(0.29)
π*C14-C15	0.15948	C14	48.95	S(00.00)+P(99.94)+D(0.06)
		C15	51.05	S(00.00)+P(99.94)+D(0.06)
π*C23-C25	0.23609	C23	52.57	S(00.01)+P(99.92)+D(0.07)
		C25	47.43	S(00.00)+P(99.94)+D(0.06)

Where $\mathbf{q_i}$ is the donor orbital occupancy, $\boldsymbol{\varepsilon_i}$, and $\boldsymbol{\varepsilon_j}$ are diagonal elements (orbital energies), and F^2 (i, j) is the off-diagonal Fock matrix element. The data presented in Table 4 (a-b) for the derivatives 6MNPM and 4NPMB show that the correspondence between the bonding donor (C_{26}-C_{27}) and anti-bonding acceptor (C_{24}-C_{25}) has a maximum stabilizing energy value of 20.25 Kcal mol^{-1} for the 6MNPM molecule.

Table 4(a). Second-order perturbation theory analysis of Fock matrix in NBO basic for 6MNPM molecule with the basic set 6-311++G (d, p).

Donor(i)	Type of bond	Acceptor(j)	Type of bond	$\boldsymbol{E^2}$ $(\boldsymbol{kJ}/\text{mol})^a$	E(j) - E(i) (a.u)[b]	F(i.j) (a.u)[c]
C1-C5	σ	C4-C5	σ*	01.91	1.29	0.044
C1-O14	σ	C2-C7	σ*	02.51	1.21	0.049
C1-O15	π	C1-O15	π*	00.61	0.35	0.014
	π	C4-C5	π*	04.91	0.39	0.040
C2-C3	π	C4-C5	π*	10.58	0.32	0.053
		C7-C11	π*	10.04	0.31	0.049
C4-C5	π	C1-O15	π*	16.56	0.28	0.062
		C2-C3	π*	09.14	0.31	0.050
C7-C11	π	C2-C3	π*	10.24	0.30	0.051
		C8-C10	π*	10.65	0.31	0.052
C8-C10	π	C7-C11	π*	10.26	0.31	0.050
C24-C25	π	C23-C28	π*	12.02	0.30	0.054
C26-C27	π	C24-C25	π*	20.45	0.18	0.060
N33-O35	π	C26-C27	π*	01.14	1.48	0.037

Table 4(b). Second order perturbation theory analysis of Fock matrix in NBO basic for 4NPMB molecule with the basic set 6-311++G (d, p).

Donor(i)	Type of bond	Acceptor(j)	Type of bond	$\boldsymbol{E^2}$ $(\boldsymbol{kJ}/\text{mol})^a$	E(j) - E(i) (a.u)[b]	F(i.j) (a.u)[c]
C1-C6	π	C2-C3	π*	11.16	0.30	0.052
C2-C3	π	C1-C6	π*	09.89	0.31	0.050
C2-H19	σ	C3-C4	σ*	05.51	0.94	0.064

C4-C5	π	C14-C15	π*	10.01	0.30	0.051
		C7-C13	π*	11.04	0.29	0.051
C7-C13	π	C4-C5	π*	10.32	0.33	0.053
		C14-C15	π*	09.15	0.32	0.049
C8-C9	π	C7-C13	π*	09.32	0.31	0.050
C12-O21	π	C12-O21	π*	00.63	0.35	0.014
		C8-C10	π*	04.85	0.39	0.040
C14-C15	π	C4-C5	π*	09.63	0.32	0.051
		C7-C13	π*	10.88	0.30	0.052
C23-C25	π	C27-C28	π*	13.18	0.30	0.057
C27-C28	π	N29-O31	π*	20.80	0.18	0.060
N29-O31	π	C27-C28	π*	03.64	0.48	0.040

The 4NPMB molecule has the highest stabilization energy value of 20.80 Kcal mol^{-1} between the bonding donor of (C_{27}-C_{28}) and the anti-bonding acceptor of (N_{29}-O_{31}). The interactions mentioned above represent the most significant interactions of coumarin derivatives among all interactions.

3.6 Polarizability and hyperpolarizability (NLO)

The polarizability tensor components' value depends on the chosen Cartesian coordinate system. Isotropic derivatives have the same polarizability in all directions, while anisotropic derivatives have different directions. Raman scattering intensity is proportional to derived polarizability components, which are constant regardless of the molecules' orientation. The quantities ($\bar{\alpha}$) and (γ) measure the scattering intensity and anisotropy invariant, respectively. Using the DFT chemical model with a basis set of B3LYP/6-311++G (d, p) numerical derivative of the dipole moment, the polarizability invariant is calculated. Table 5 displays the relevant parameter values. There are atomic units in the calculated values. Accordingly, the computed values are transformed into electrostatic units (for β, 1 a.u. = 8.6393 x 10^{-33} esu, and for α, 1 a.u. = 0.1482 x 10^{-24} esu). Definitions [43] about isotropic polarizability state that

$$\bar{\alpha} = 1/3(\alpha_{xx} + \alpha_{yy} + \alpha_{zz})$$

The polarizability anisotropy invariant is

$$\gamma^2 = 1/2\left[(\alpha_{xx} - \alpha_{yy})^2 + (\alpha_{yy} - \alpha_{zz})^2 + (\alpha_{zz} - \alpha_{xx})^2 + 6(\alpha_{xy}^2 + \alpha_{yz}^2 + \alpha_{zx}^2)\right]$$

and the average hyperpolarizability is

$$\beta_{total} = \sqrt{(\beta_x^2 + \beta_y^2 + \beta_z^2)}$$

or

$$\beta_{total} = \sqrt{(\beta_{xxx} + \beta_{xyy} + \beta_{xzz})^2 + (\beta_{yyy} + \beta_{yxx} + \beta_{yzz})^2 + (\beta_{zzz} + \beta_{zxx} + \beta_{zyy})^2}$$

where α_{xx}, α_{yy} and α_{zz} are elements of the polarizability tensor. β_x, β_y *and* β_z are hyperpolarizability's tensor components. The study of NLO of coumarin derivatives will provide useful information that could be used to understand important properties like optoelectronic applications. Table 5 provides the parameters of 6MNPM and 4NPMB molecules.

Table 5. Total electric dipole moment ($\bar{\mu}$), the mean polarizability($\bar{\alpha}$), the anisotropy polarizability ($\bar{\gamma}$), and mean first-order hyperpolarizability with the basic set 6-311++G (d, p).

Parameters	DFT	
	6MNPM	4NPMB
Electric dipole moment ($\bar{\mu}$)		
μ_x	0.93	2.93
μ_y	3.31	4.20
μ_z	0.04	-0.43
$\bar{\mu}$ (Debye)	3.44	5.15
Polarizability(α)		
α_{xx}	-186.58	-186.80
α_{yy}	-132.66	-156.00
α_{zz}	-140.89	-145.59
α_{xy}	027.78	033.18
α_{xz}	000.98	004.71
α_{yz}	-004.95	-001.17
$\bar{\alpha}$	-153.38	-162.80
$\bar{\gamma}$	379.98	403.56
$\bar{\alpha}$ esu (x 10^{-24})	-022.73	-024.12
$\bar{\gamma}$ esu (x 10^{-24})	056.31	059.80
Hyperpolarizability(β)		
β_{xxx}	324.19	380.23
β_{yyy}	110.48	119.40
β_{zzz}	-002.23	000.60
β_{xyy}	-084.13	-061.98
β_{xxy}	048.18	027.77
β_{xxz}	-033.90	-052.49
β_{xzz}	-017.99	-028.20
β_{yzz}	-013.05	-022.92
β_{yyz}	006.25	-009.28
β_{xyz}	-009.41	-007.53
β_x	222.07	290.04
β_y	145.61	124.25
β_z	-029.88	-061.17
β_{total}	267.23	321.41
β_{total} esu (x 10^{-33})	2308.70	2776.78

It included the values of electric dipole moment, polarizability and hyperpolarizability of coumarin molecules. The 4NPMB molecule has a slightly larger value of parameters mentioned above as compared to the 6MNPM molecule.

3.7 Thermodynamic Properties

Using DFT as a chemical model and the B3LYP/6-311++G (d, p) basis set, the values for various thermodynamic parameters, such as heat capacity, entropy, and enthalpy changes of the title molecule in the gas phase at different temperatures are computed to explain, how the thermodynamic parameters change while changing the chemical models. These thermodynamic parameters are rising with temperatures between 100 and 1000K, as shown in Table 6, because molecule vibrational intensities are increasing with temperature [43]. Figure 6 shows how entropy (S), enthalpy change (ΔHo→T), and heat capacity at constant pressure (Cp) relate to temperature. It reveals that the thermal energy and entropy of the 6MNPM molecule are the same at the temperature of 400K, while 4NPMB molecule requires 470 K to achieve the same state. This difference in temperature is likely due to the distinct molecular structures of the two coumarin molecules.

Table 6. Thermodynamic properties of 6MNPM and 4NPMB molecules at different temperatures by B3LYP/6-311++G (d, p).

Temperature (k)	C_v (calmol^{-1}K^{-1})		S (calmol^{-1}K^{-1})		ΔH_o (calJmol^{-1})	
	6MNPM	4NPMB	6MNPM	4NPMB	6MNPM	4NPMB
100	34.10	32.50	100.59	99.62	163.81	173.83
200	56.26	56.09	132.37	130.61	168.32	178.23
273	73.06	74.55	152.96	151.39	173.04	183.00
298	78.85	80.89	159.83	158.41	174.95	184.96
300	79.28	81.35	160.33	158.93	175.09	185.11
400	101.00	105.02	186.75	186.22	184.13	194.45
500	119.47	125.04	211.78	212.32	195.18	205.99
600	134.53	141.31	235.30	236.97	207.91	219.33
700	146.71	154.43	257.30	260.08	222.00	234.14
800	156.60	165.05	277.82	281.69	237.18	250.14
900	164.68	173.70	296.98	301.88	253.26	267.09
1000	171.34	180.81	314.90	320.77	270.07	284.83

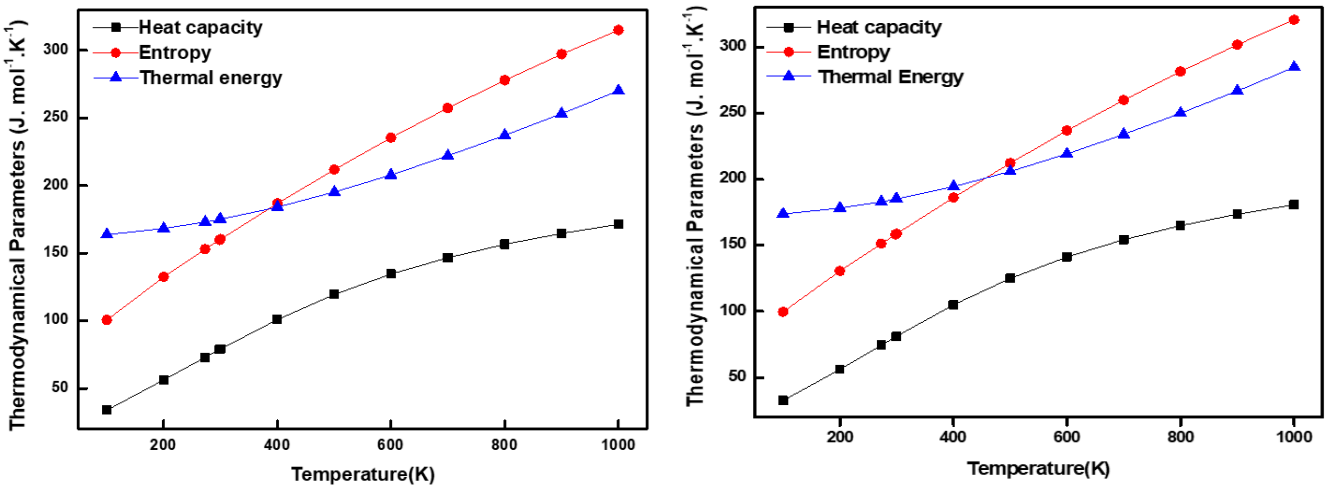

(a) (b)

Fig 6. Correlation Graph of (a) 6MNPM and (b) 4NPMB molecules.

4. Conclusion

In the current work, the thermal properties of both derivatives were analysed together with the geometrical characteristics of the optimal structure of coumarin molecules. The MEP map demonstrates that the positive potential sites are located around the N and H atoms connected to the benzene ring, while the negative potential sites are located around the O atom related to the C. Analysis of natural bond orbitals reveals the strong intramolecular interactions. The HOMO and LUMO reveal the molecule's chemical activity. Utilizing the orbital energies, molecular traits like electronegativity, chemical potential, hardness, softness, and electrophilicity index were calculated. The reduction of the HOMO-LUMO energy band gap supports the molecule's bioactive properties. The Mulliken charges and first-order hyperpolarizability are determined. Since

molecular vibration intensities increase with temperature, thermodynamic characteristics show that heat capacities, entropies and enthalpies essentially rise with temperature. We intend that all the computed and analysed data above will be helpful to future researchers.

Acknowledgments: The authors are thankful to the Photophysical lab for providing the Gaussian Windows 16 software for theoretical calculation at the Department of Physics, Gulbarga University, Kalaburagi -06.

Author Contributions: Each author contributed to the idea and planning of the study. Srinath, Omnath Patil, Shivakumar Chillargikar, Dayanand Lalasangi and S. M. Hanagodimath prepared the materials, collected the data, and conducted the analysis. All contributors provided feedback on earlier iterations of the article, with Srinath writing the original draft. The final manuscript was reviewed and approved by each author.

Funding: The authors affirm that no funding, money, or other assistance was obtained in order to prepare this work.

Data Availability: During the current investigation, no datasets were created; only the occurred data.

Declarations

Competing Interests: None of the authors has any conflicting interests.

References

[1] M. A. Musa, J. S. Cooperwood, and M. O. Khan, "A review of coumarin derivatives in pharmacotherapy of breast cancer," Curr. Med. Chem., vol. 15, pp. 2664–2679, 2008.

[2] F. Borges, F. Roleira, N. Milhazes, L. Santana, and E. Uriarte, "Simple coumarins and analogues in medicinal chemistry: Occurrence, synthesis and biological activity," Curr. Med. Chem., vol. 12, pp. 887–916, 2005.

[3] G. R. Geen, J. M. Evens, A. K. Vong, A. R. Katritzky, C. W. Rees, and E. F. V. Scriven, "Pyrans and their benzo derivatives: Applications," in Comprehensive Heterocyclic Chemistry II, R. Lan, C. W. R. Katritzky, and E. F. V. Scriven, Eds. Oxford, U.K.: Pergamon Press, 1997, pp. 469–500.

[4] D. Egan, R. O'Kennedy, E. Moren, D. Cox, E. Prosser, and R. D. Thornes, "The pharmacology, metabolism analysis and applications of coumarin and coumarin-related compounds," Drug Metab. Rev., vol. 22, pp. 503–529, 1990.

[5] M. Curini, G. Cravotto, F. Epifano, and G. Giannone, "Chemistry and biological activity of natural and synthetic phenyloxy coumarins," Curr. Med. Chem., vol. 13, pp. 199–222, 2006.

[6] P. Anand, B. Singh, and N. Singh, "A review on coumarins as acetylcholinesterase inhibitors for Alzheimer's disease," Bioorg. Med. Chem., vol. 20, pp. 1175–1180, 2012.

[7] X. Liu, J. M. Cole, P. G. Waddell, T. C. Lin, J. Radia, and A. Zeidler, "Molecular origins of optoelectronic properties in coumarin dyes: Toward designer solar cell and laser application," J. Phys. Chem. A, vol. 116, pp. 727–737, 2011.

[8] K. P. Barot, S. V. Jain, L. Kremer, S. Singh, and M. D. Ghate, "Recent advances and therapeutic journey of coumarins: Current status and perspectives," Med. Chem. Res., vol. 24, pp. 2771–2798, 2015.

[9] G. L. Delogu and M. J. Matos, "Coumarins as promising scaffold for the treatment of age-related diseases—An overview of the last five years," Curr. Top. Med. Chem., vol. 17, pp. 3173–3189, 2017.

[10] A. G. Pramod, C. G. Renuka, and Y. F. Nadaf, "Electronic structure, optical properties and quantum chemical investigation on synthesized coumarin derivative in liquid media for optoelectronic devices," J. Fluorescence, vol. 29, pp. 953–968, 2019.

[11] W. Kohn, "Nobel Lecture: Electronic structure of matter—Wave functions and density functionals," Rev. Mod. Phys., vol. 71, pp. 1253–1266, 1999.

[12] I. Azad, Y. Akhter, T. Khan, M. I. Azad, S. Chandra, P. Singh, D. Kumar, and M. Nasibullah, "Synthesis, quantum chemical study, AIM simulation, in silico ADMET profile analysis, molecular docking and antioxidant activity assessment of aminofuran derivatives," J. Mol. Struct., vol. 127, pp. 285, 2019.

[13] E. Molteni, G. Cappellini, G. Onida, and G. Mula, "Extensive stacking of DHI-like monomers as a model of out-of-plane complexity in eumelanin protomolecules: Chemical and structural sensitivity of optical absorption spectra," Chem. Phys., vol. 524, pp. 92–100, 2019.

[14] D. Zhao, Q. Lu, R. Su, Y. Li, and M. Zhao, "Light harvesting and optical-electronic properties of two quercetin and rutin natural dyes," Appl. Sci., vol. 9, no. 2567, 2019.

[15] M. A. L. Marques and E. K. U. Gross, "Time-dependent functional theory," Annu. Rev. Phys. Chem., vol. 55, pp. 427–455, 2004.

[16] K. V. Basavarajappa, Y. Arthoba Nayaka, H. T. Purushothama, M. M. Vinaya, A. Antony, and P. Poornesh, "Optoelectronic and current-voltage studies for novel coumarin dyes," Int. J. Environ. Anal. Chem., pp. 1–14, 2019.

[17] K. Hara, T. Sato, R. Katoh, A. Furube, Y. Ohga, A. Shinpo, S. Suga, K. Sayama, H. Sugihara, and H. Arakawa, "Molecular design of coumarin dyes for efficient dye-sensitized solar cells," J. Phys. Chem. B, vol. 107, pp. 597–606, 2003.

[18] C. I. Oprea, P. Panait, F. Cimpoesu, M. Ferbinteanu, and M. A. Girtu, "Density functional theory (DFT) study of coumarin-based dyes absorbed on TiO2 nanoclusters—Applications to dye-sensitized solar cells," Materials, vol. 6, pp. 2372–2392, 2013.

[19] K. Hara, Z. S. Wang, T. Sato, A. Furube, R. Katoh, H. Sugihara, Y. Danoh, C. Kasad, A. Shinpo, and S. Suga, "Oligothiophene-containing coumarin dyes for efficient dye-sensitized solar cells," J. Phys. Chem. B, vol. 109, pp. 15476–15482, 2005.

[20] R. Sanchez-de-Armas, M. A. San Miguel, J. Oviedo, and J. F. Sanz, "Coumarin derivatives for dye-sensitized solar cells: A TD-DFT study," Phys. Chem., vol. 14, pp. 225–233, 2012.

[21] F. Mutlak, A. Mohi, and T. Alwan, "Density functional theory study of molecular structure, electronic properties, UV-Vis spectra on coumarin 102," Baghdad Sci. J., vol. 13, pp. 143–152, 2016.

[22] Srinath, D.Lalasangi, V.Mallayya*, S. M. Hanagodimath "Fluorescence Quenching Analysis of 6MNPM Molecule by Steady State Method". g analysis of 6MNPM molecule Mapana – Journal of Sciences 2025, Vol. 24, No. 1, 43-52 ISSN 0975-3303.

[23] M. Basanagouda, M. V. Kulkarni, D. Sharma, V. K. Gupta, P. Pranesha, P. Sandhyarani, and V. P. Rasal, "Synthesis and biological evaluation of some novel 1,2,4-triazole derivatives," J. Chem. Sci., vol. 121, pp. 485–495, 2009.

[24] A. Kumar, G. Cappellini, and F. Delogu, "Electronic and optical properties of chromophores from hexaneuronic acids," Cellulose, vol. 26, pp. 1489–1501, 2019

[25] N. Chowdareddy, A. R. Lamani, A. G. Pramod, and V. B. Tangod, "Nonlinear refractive index enhancement of Nd^{3+} ions loaded borate glasses in the near-infrared region by silver nanoparticles," Opt. Mater., vol. 142, p. 114067, 2023.

[26] V. B. Tangod, B. M. Mastiholi, P. Raikar, S. G. Kulkarni, and U. S. Raikar, "Studies of the photophysics of highly fluorescent Red Mega 480 laser dye in solutions: Steady state spectroscopy," Spectrochim. Acta A Mol. Biomol. Spectrosc., vol. 148, pp. 105–113, 2015.

[27] M. S. Jadhav, L. S. Laxmeshwar, J. F. Akki, P. U. Raikar, V. B. Tangod, and U. S. Raikar, "Multimode fiber optic sensor for adulterant traces in edible oil using nanotechnology technique," Mater. Today Proc., vol. 4, no. 11, pp. 11910–11914, 2017.

[28] S. Patil, O. Devar, and S. Srinath, "Estimation of electric dipole moment by solvatochromism, computational method, and study of the effect of solvents by preferential solvation of 6-methoxy-4-(4-nitro-phenoxy methyl)-chromen-2-one (6MNPM)," J. Fluoresc., 2024.

[29] X. Liu, J. M. Cole, and K. S. Low, "Solvent effects on the UV-Vis absorption and emission of optoelectronic coumarins: A comparison of three empirical solvatochromic models," J. Phys. Chem. C, vol. 117, pp. 14731–14741, 2013.

[30] A. G. Pramod, C. G. Renuka, Y. F. Nadaf, and R. Rajaramakrishna, "Impact of solvents on energy gap, photophysical, photometric properties for a new class of 4-HCM coumarin derivative: Nonlinear optical studies and optoelectronics applications," J. Mol. Liq., vol. 292, pp. 111–393, 2019.

[31] M. Cossi, J. M. Millam, M. Klene, C. Adamo, R. Cammi, J. W. Martin, D. J. Fox, Gaussian 09, Revision D.01, Gaussian Inc., Wallingford, CT, 2009.

[32] M. A. Mumit, T. K. Pal, M. A. Alam, M. A. Islam, S. Paul, M. C. Sheikh, "DFT studies on vibrational and electronic spectra, HOMO-LUMO, MEP, HOMO, NBO and molecular docking analysis of benzyl-3-N-(2,4,5-trimethoxyphenylmethylene) hydrazinecarbodithioate," J. Mol. Struct., vol. 1220, p. 128715, 2020.

[33] V. Q. Vuong, Y. Nishimoto, D. G. Fedorov, B. G. Sumpter, T. A. Niehaus, and S. Irle, "The fragment molecular orbital method based on long-range corrected," J. Chem. Theory Comput., vol. 15, no. 5, pp. 3008–3020, 2019.

[34] V. K. Choudhary, K. Bhatt, D. Dash, and N. Sharma, "DFT calculation on molecular structure, HOMO-LUMO study, reactivity descriptors and spectral analysis of newly synthesized diorganotin (IV) 2-chloridophenylacetohydroxamate complexes," J. Comput. Chem., vol. 40, no. 27, pp. 2354–2363, 2019.

[35] S. Muthu and E. I. Paulraj, "Molecular structure, vibrational spectra, first order hyperpolarizability, NBO and HOMO-LUMO analysis of 4-amino-3(4-chlorophenyl)butanoic acid," Solid State Sci., vol. 14, no. 4, pp. 476–487, 2012.

[36] J. Frau, F. Muñoz, and D. Glossman-Mitnik, "Validation of Koopman's theorem in DFT through the calculation of the conceptual DFT descriptors of three fluorescent DNA staining dyes," Chem. Informatics, vol. 2, no. 2, 2016.

[37] A. U. Rani, N. Sundaraganesen, M. Kurt, M. Cinar, and M. Karabacak, "FT-IR, FT-Raman, NMR spectra and DFT calculation on 4-chloro-N-methylaniline," Spectrochim. Acta Part A Mol. Biomol. Spectrosc., vol. 75, no. 5, pp. 1523–1529, 2010.

[38] S. P. Vijayachamundeshwari, E. J. Jebaseelen Samuel, and N. Sundaraganesan, "Molecular structure, vibrational spectra, NMR and UV spectral analysis of sulfamethoxazole," Spectrochim. Acta Part A Mol. Biomol. Spectrosc., vol. 118, pp. 1–10, 2014.

[39] A. E. Reed, R. B. Weinstock, and F. Weinhold, "J. Chem. Phys.," vol. 83, pp. 735–743, 1985.

[40] A. E. Reed and F. Weinhold, "J. Chem. Phys.," vol. 83, pp. 1736–1747, 1985.

[41] A. E. Reed and F. Weinhold, "J. Chem. Phys.," vol. 78, pp. 4066–4072, 1983.

[42] F. Weinhold and C. R. Landis, Discovering Chemistry with Natural Bond Orbitals, John Wiley & Sons, New Jersey, 2012.

[43] R. J. Xavier and A. Prabaharan, "Vibrational spectroscopic investigations of 4,4-dimethyl-2-oxazoline: A density functional theory approach," Spectrochimica Acta Part A: Molecular and Biomolecular Spectroscopy, vol. 136, pp. 1530–1542, 2015.